MEM APPLICATION TO IRAS CPC IMAGES

A. P. MARSTON
Dept. of Physics & Astronomy, Drake University, Des Moines, IA 50311

ABSTRACT A method for applying the Maximum Entropy Method (MEM) to Chopped Photometric Channel (CPC) IRAS additional observations is illustrated. The original CPC data suffered from problems with repeatability which MEM is able to cope with by use of a noise image, produced from the results of separate data scans of objects. The process produces images of small areas of sky with circular Gaussian beams of approximately 30″ full width half maximum resolution at 50 and 100μm. Comparison is made to previous reconstructions made in the far-infrared as well as morphologies of objects at other wavelengths. Some projects with this dataset are discussed.

INTRODUCTION

The Chopped Photometric Channel (CPC) instrument was part of the Dutch Auxiliary instrument package on IRAS. It produced simultaneous 50 and 100μm raster scan, pointed observations of small areas (9′ x 9′) of the sky. Generally, objects covered by these scans were observed more than once. The original resolution of these images is 88″ at 50μm and 100″ at 100μm and beams were close to circular gaussians (Wesselius *et al.* 1986). They had the best "raw" resolution of any IRAS data set at these wavelengths. In all, approximately 3000 images of 1000 objects in the two wavebands were made including over 300 galaxies. There were a number of problems with images produced:

i) Major (and minor) glitching in the images. (These were removed in an off-line process performed in Groningen).

ii) Small sky coverage leading to problems in the calibration.

iii) Repeatability of (in particular) faint features was low.

In using a CPC image we are starting with a high resolution image and would therefore expect to recover the highest resolutions of any IRAS product after applying MEM. Keeping in mind the noise problems experienced by the CPC detectors, the fact that MEM reconstructs an image which is not an overinterpretation of the original data, i.e. that is reasonable given the noise across the image, is an important part of the image reconstruction.

METHOD OF APPLICATION

The flow chart shown in Figure 1 illustrates the procedure used in the MEM reconstruction of a CPC image. Only objects for which two or more CPC observations exist were used. Reconstructions were halted when the global χ^2 fit

S. Terebey and J. Mazzarella (eds.), *Science with High-Spatial Resolution Far Infrared Data*, 11–16, 1994, Jet Propulsion Laboratory, Pasadena, CA.

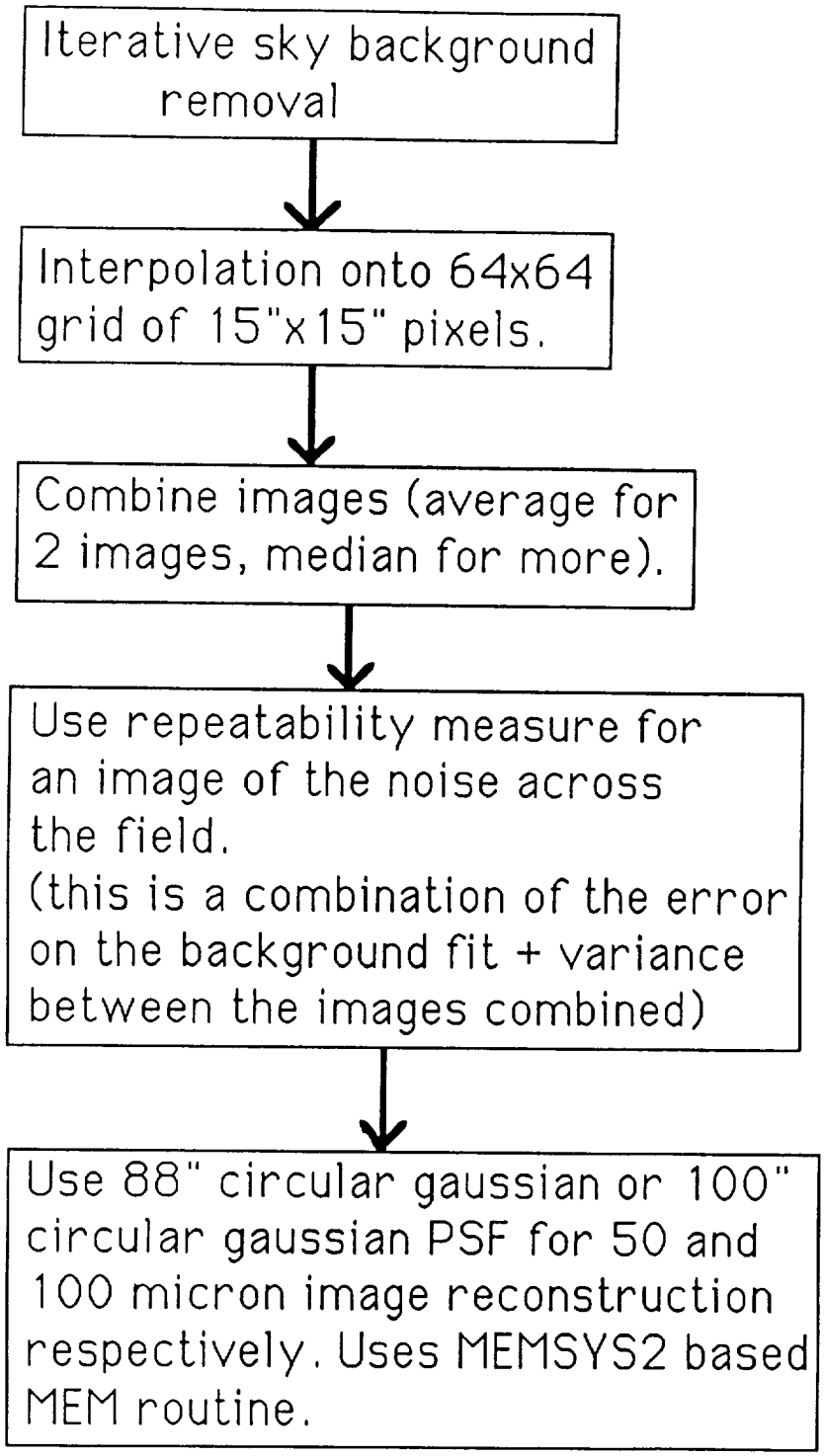

FIGURE 1 Flow chart outlining the procedure used in the MEM reconstructions of CPC images.

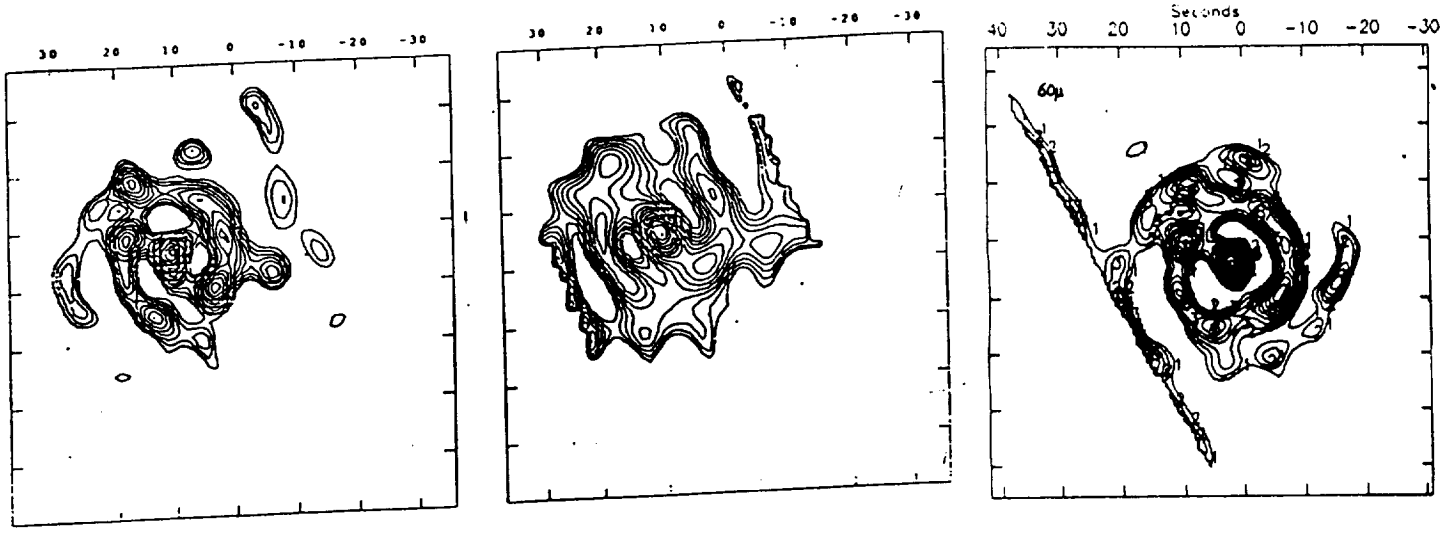

FIGURE 2 The 50 and 100μm MEM reconstruction images of M83 (left and center respectively) from the CPC data compared with the DSD 60μm reconstruction of Marston (1989) to the right.

of the image reconstruction compared to the original data equalled 1.0 per pixel or after 20 iterations of the MEM routine (for details on the background fitting and noise maps see Marston 1992a).

RESULTS AND COMPARISON TO PREVIOUS WORK

Morphological features produced in the reconstructions were compared to features seen in previous reconstructions for M83 and M51 (Marston 1989; Canterna *et al.* 1990). The M83 example is shown in Figure 2. The CPC reconstructions show very similar features to the reconstructed IRAS DSD AO produced by Marston (1989). Comparisons to features observed in other wavebands were also used as secondary indicators of the reliability of the reconstructed images (see Figure 6 of Marston 1989). A reconstruction of a point source image indicated a resolution of 24″ was typically achieved at both 50 and 100μm.

Limitations of the data

Some limitations exist on the reconstruction. Objects need to be smaller than 9′ across to fit within the raster scans of the CPC. Noise exists at the edge of the arrays where the individual raster scans, combined to create the final image of an object, do not precisely overlap. Features below 5MJy/sr (typically) are unreliable (this is a 3σ value for noise at the sky level on the combined maps).

DATA USES

A number of topics have been investigated or are under investigation using MEM processed CPC images.

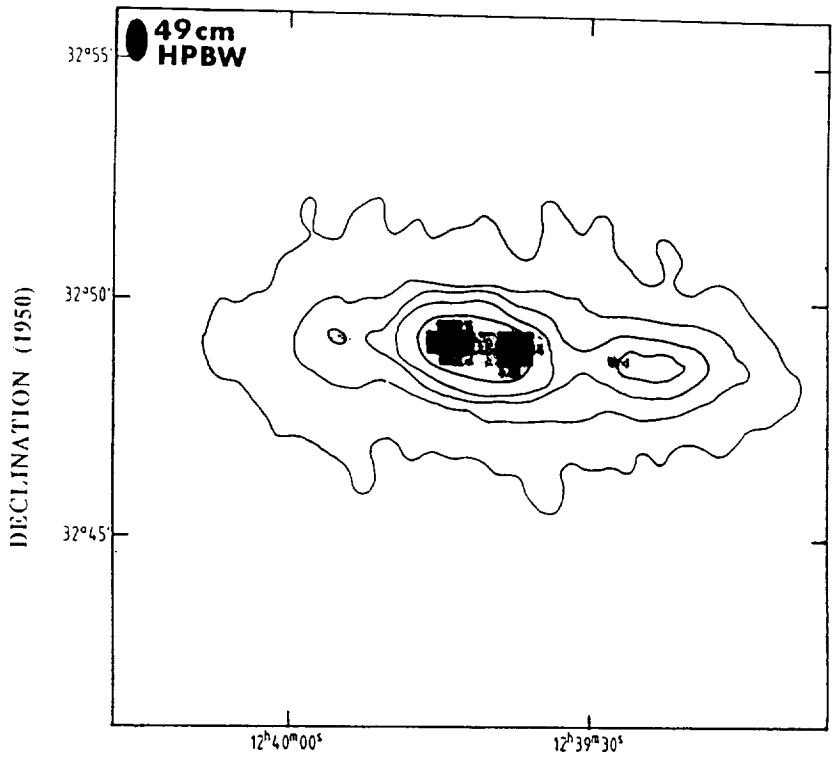

FIGURE 3 A greyscale image of the reconstructed 50μm image of the edge-on spiral NGC 4631 with contours of the 49cm non-thermal radio emission overlaid (Werner 1985). A distinct spatial correlation is evident between the features seen in both the radio and far-infrared.

Extended Far-Infrared Emission in Active Galaxies

The nearby radio galaxy, Centaurus A, shows a warped dust disk structure in reconstructed images (see Marston 1992b). Emission follows the Hα distribution shown in the TAURUS data of Bland et al. (1987). Regions of Hα line-splitting are coincident with peaks seen in the 50μm image. A sample of CPC images of Seyfert galaxies have been investigated in order to investigate the relation of the active nucleus in these galaxies to the far-infrared emission (Marston 1992a; Marston 1993). These show that many nearby Seyfert galaxies have extended regions of FIR emission which can often be resolved into RdiskS and RbulgeS components (e.g., NGC 7582).

Detailed correlation of far-infrared and radio features

Recent work by Bicay and Helou (1990) and Helou and Bicay (1993) have indicated that the strong non-thermal radio – far-infrared correlation shown in the global fluxes of galaxies also exists as a strong spatial correlation inside the galaxies. To investigate this further, the MEM processed images allow a more detailed comparison. An example of this is NGC 4631 (Figure 3). The spatial relation between features is excellent. However, the far-infrared peaks compared

FIGURE 4 Contours of the IRAS 50μm image overlaid on a greyscale production of an R band CCD frame of Arp 270. The extended far-infrared emission associated with each of the galaxies is evident and they are clearly separated. The apparent distance between the nuclei of the two galaxies is 80″.

to the far-infrared background are stronger by a factor of 3 than the corresponding radio peaks compared to the radio background in this galaxy. This would suggest these areas are the source of the fast charged particles needed for the radio emission, the charged particles having now leaked away from these sources.

Interacting galaxies

Preliminary investigations have so far been made into separating the far-infrared emission associated with pairs and groups of interacting galaxies (see the example of Arp 270 in Figure 4). This allows the determination of the effect that interactions have on the star formation processes in these interactions (see e.g. Surace *et al.* 1993). The example in Figure 4 shows how Arp 270 has been easily split into the two components associated with the galaxies NGC 3995 and NGC 3996.

Classification of edge-on spiral galaxies

The existence of the far-infrared knots seen in the reconstructed CPC image of NGC 4631, shown in Figure 3, suggest they are due to the perspective of viewing along the edge of a spiral arm of this edge-on disk galaxy. The spacing between the arms, indicated by the far-infrared peaks, should allow the arm class classification of this galaxy and may also be applied to reconstructions of other edge-on spirals.

CONCLUSION

A method of reconstructing far infrared images at 50 and 100μm at 30″ resolution from the IRAS CPC database has been illustrated. The reconstructed beams are circular Gaussians. Reliable reconstructions of objects $< 9'$ across have been obtained. The CPC database contains a number of galaxies, and these may be used for the study of distributed far-infrared emission from active galaxies, star formation in interacting galaxies and groups, the far-infrared/non-thermal radio correlation in galaxies and spiral arm classification of edge-on spirals.

REFERENCES

Bicay, M. D., and Helou, G. 1990, *ApJ*, **362**, 59

Bland, J., Taylor, K., and Atherton, P. D. 1987, *MNRAS*, **228**, 595

Canterna, R., Hackwell, J. A., and Grasdalen, G. L. 1990, In *Proceedings of the Second Wyoming Conference: The Interstellar Medium in External Galaxies, Summaries of Contributed Papers*, eds. D. J. Hollenbach and H. A. Thronson Jr., NASA Conference Publication 3084, p. 301

Helou, G., and Bicay, M. D. 1993, *ApJ*, **415**, 93

Marston, A. P. 1989, *AJ*, **98**, 1572

Marston, A. P. 1992a, In *Relationships Between Active Galactic Nuclei and Starburst Galaxies*, ed. A. V. Filippenko, ASP Conference Series, Vol. 31, p.117

Marston, A. P., 1992b, In *Relationships Between Active Galactic Nuclei and Starburst Galaxies*, ed. A. V. Filippenko, ASP Conference Series, **31**, p.123

Marston, A. P. 1993, in *Proceedings of the Workshop on Science with High Spatial Resolution Far-Infrared Data*, JPL, pp. 89-95

Surace, J. A., Mazzarella, J. M., Soifer, B. T., and Wehrle, A. E. 1993, *AJ*, **105**, 864

Werner, W. 1985, *A&A*, **144**, 502

Wesselius, P. R., Beitema, D. A., de Jonge, A. R. W., Jurriens, T. A, Kester, D. J. M., van Weerden, J. E., de Vries, J., and Perault, M. 1986, *IRAS-DAX Chopped Photometric Channel, Explanatory Supplement* (Groningen: Laboratory for Space Research)